

Transmission Geometry Laser Desorption Atmospheric Pressure Photochemical Ionization Mass Spectrometry for Analysis of Complex Organic Mixtures

Leonard Nyadong,^{†,||} Mmili M. Mapolelo,^{†,⊥} Christopher L. Hendrickson,^{†,‡,§} Ryan P. Rodgers,^{*,†,‡,§} and Alan G. Marshall^{*,†,‡,§}

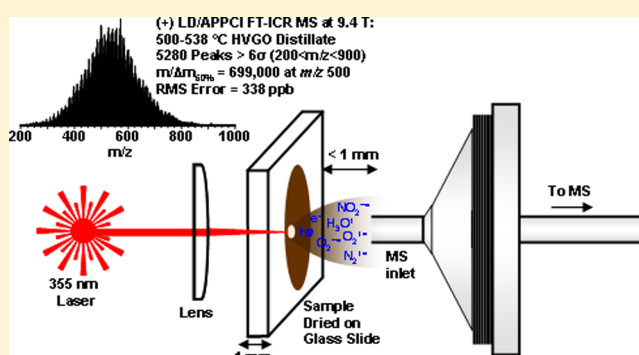
[†]National High Magnetic Field Laboratory, Florida State University, 1800 East Paul Dirac Drive, Tallahassee, Florida 32310, United States

[‡]Department of Chemistry and Biochemistry, Florida State University, 95 Chieftain Way, Tallahassee, Florida 32303, United States

[§]Future Fuels Institute, Florida State University, 1800 East Paul Dirac Drive, Tallahassee, Florida 32310, United States

Supporting Information

ABSTRACT: We present laser desorption atmospheric pressure photochemical ionization mass spectrometry (LD/APPCI MS) for rapid throughput analysis of complex organic mixtures, without the need for matrix, electric discharge, secondary electrospray, or solvents/vaporizers. Analytes dried on a microscope slide are vaporized in transmission geometry by a laser beam aligned with the atmospheric pressure inlet of the mass spectrometer. The laser beam initiates a cascade of reactions in the region between the glass slide and MS inlet, leading to generation of reagent ions for chemical ionization of vaporized analyte. Positive analyte ions are generated predominantly by proton transfer, charge exchange, and hydride abstraction, whereas negative ions are generated by electron capture or proton transfer reactions, enabling simultaneous analysis of saturated, unsaturated, and heteroatom-containing hydrocarbons. The absence of matrix interference renders LD/APPCI MS particularly useful for analysis of small molecules (<2000 Da) such as those present in petroleum crude oil and petroleum deposits. $[M + H]^+$ and $M^{+\bullet}$ dominate the positive-ion mass spectra for olefins and polyaromatic hydrocarbons, whereas saturated hydrocarbons are observed mainly as $[M - H]^+$ and/or $M^{+\bullet}$. Heteroatom-containing hydrocarbons are observed predominantly as $[M + H]^+$. $[M - H]^-$ and $M^{-\bullet}$ are the dominant negative ions observed for analytes of lower gas-phase basicity or higher electron affinity than O_2 . The source was coupled with a 9.4 T Fourier transform ion cyclotron resonance mass spectrometer (FTICR MS) to resolve and identify thousands of peaks from Athabasca bitumen heavy vacuum gas oil distillates (400–425 and 500–538 °C), enabling simultaneous characterization of their polar and nonpolar composition. We also applied LD/APPCI FTICR MS for rapid analysis of sodium and calcium naphthenate deposits with little to no sample pretreatment to provide mass spectral fingerprints that enable reliable compositional characterization.



Laser desorption/ionization (LDI) techniques play an increasingly important role in advances of modern mass spectrometry for high-resolution surface analysis.¹ Matrix-assisted laser desorption ionization (MALDI), which commonly uses an ultraviolet laser for analyte desorption and ionization, has greatly broadened the scope of biological applications of mass spectrometry with key contributions in proteomics, glycomics, and lipidomics.^{2–4} Atmospheric pressure (AP/MALDI)⁵ MALDI is advantageous for studying highly fragile biomolecules, e.g., phosphopeptides,⁶ because the generated ions are more efficiently thermalized by collisions with atmospheric gases, thereby minimizing fragmentation. A variant of AP/MALDI with laser interrogation of the sample in transmission geometry to generate multiply charged electrospray-like ions from peptide/proteins in the absence of electric

fields, laserspray ionization (LSI), has also been reported.⁷ However, AP/MALDI techniques generate abundant matrix and matrix–analyte cluster ion signals and also suffer from relatively poor ion transfer efficiency from source to mass analyzer, which results in lower overall signal magnitude.⁸ Interference from matrix cluster ion signals in the low-mass range ($m/z < 700$) limits the applicability of MALDI-based techniques for analysis of small molecules.

Matrix-free desorption/ionization from silicon (DIOS) has been reported as an effective technique for analysis of small molecules: the silicon substrate reportedly serves to absorb the

Received: June 10, 2014

Accepted: October 8, 2014

Published: October 27, 2014

UV laser light for reduced analyte fragmentation.⁹ However, DIOS requires special procedures such as chemical vapor deposition and electrochemical etching for preparation of the expensive silicon substrates. Moreover, the percolation of analytes into tiny pores on the silicon substrate limits laser vaporization efficiency, resulting in lower signal magnitude and poor reproducibility.¹⁰

Direct laser desorption/ionization in vacuum in the absence of matrix has been heavily explored on a variety of different surfaces for analysis of small molecules, but is not widely used due to molecular degradation upon exposure to laser light.^{9,11,12} LDI is more desirably performed at atmospheric pressure so that the vaporized analytes undergo rapid collisional cooling by atmospheric buffer gases. Atmospheric pressure implementation is also faster and more convenient. However, the laser desorption/ionization event generates only a limited number of ions together with a large population of neutral species^{4,13} and poor ion transfer from the atmospheric pressure interface to the mass analyzer reduces (or even eliminates) ion signal.

Post-ionization strategies such as chemical ionization (CI), electrospray ionization (ESI), and photoionization (PI) can provide secondary ionization of laser-desorbed neutral analytes. Techniques that take advantage of CI for post-ionization include AP LD/CI^{13–15} and laser ablation metastable-induced chemical ionization (LAMICI).¹⁶ Reagent ion generation is initiated by use of a corona discharge,¹³ metastable helium,¹⁶ or ⁶³Ni β source¹⁵ with the desorbed neutral molecules generated by use of a 10.6 μm pulsed CO₂,¹³ 532 nm,¹⁵ or 2.94 μm ¹⁶ Nd:YAG laser. Techniques that employ electrospray post-ionization include laser ablation ESI (LAESI, $\lambda = 2.94 \mu\text{m}$),^{17,18} electrospray-assisted laser desorption ionization (ELDI, $\lambda = 337 \text{ nm}$),¹⁹ and a noncontact surface sampling/electrospray emitter probe used to capture laser-desorbed ($\lambda = 337 \text{ nm}$) species from a microscope slide in transmission geometry for subsequent ESI.²⁰ Electrospray post-ionization of vaporized neutral species generated by use of an intense femtosecond laser beam ($\lambda = 800 \text{ nm}$) has also been reported.²¹ Laser ablation ($\lambda = 2.94 \mu\text{m}$) has recently been coupled with photoionization by use of 10 and 10.6 eV photons produced from a radiofrequency krypton discharge vacuum ultraviolet (VUV) lamp in laser ablation atmospheric pressure photoionization (LAAPPI) for analysis of water-rich solid samples.²² Laser desorption at atmospheric pressure by use of a rigid endoscope lance for direct shockwave ablation of surface-bound analytes has been coupled with single photon (126 nm, 118 nm) post-ionization for rapid/selective detection of explosives from surfaces. Techniques that also employ photoionization at atmospheric pressure include atmospheric pressure photoionization (APPI)²³ and atmospheric pressure laser ionization (APLI),²⁴ both of which make use of a heated gas stream for thermally assisted vaporization of solution-phase analytes. APPI utilizes one-step vacuum ultraviolet photons for dopant-assisted photoionization,²⁵ whereas APLI relies on direct stepwise two-photon ionization (resonantly enhanced multiphoton ionization, REMPI) by use of a 248 nm high repetition rate excimer laser for enhanced ionization selectivity.²⁴

Here we present laser desorption atmospheric pressure photochemical ionization (LD/APPCI) in the absence of matrix, electric fields, corona discharge, secondary electrospray/photons, and solvents/vaporizers for rapid throughput analysis of small molecules such as those present in petroleum and other complex organic mixtures. Analytes dried on a microscope slide are vaporized by laser desorption in transmission

geometry with a laser beam aligned with the inlet of the mass spectrometer (MS). The laser beam also serves to generate reagent ions from atmospheric pressure buffer gases for chemical ionization of vaporized analytes. The microscope slide is positioned <1 mm from the MS inlet for efficient sampling of the generated ions to yield abundant analyte signal. We show initial results for optimization and characterization with positive and negative ions generated from various petroleum model compounds with a linear quadrupole ion trap mass spectrometer. We also coupled the ion source with an ultrahigh-resolution Fourier transform ion cyclotron resonance (FTICR) mass spectrometer to resolve and identify thousands of peaks from two Athabasca bitumen heavy vacuum gas oil distillates and to characterize crude oil sodium and calcium naphthenate deposits.

■ EXPERIMENTAL METHODS

Reagents and Sample Preparation. HPLC grade toluene (99.9%, Sigma-Aldrich, St. Louis, MO, U.S.A.) was used for dissolution/dilution of samples. Ion source optimization and characterization experiments were performed with the following petroleum model compounds: coronene, farnesene (mixture of isomers), squalene, tetradecahydroanthracene, 5- α cholestane, carbazole, perylene, benzo(ghi)perylene, tetracyclopirene, dodecyl sulfide, benzodiphenylene sulfide, dibenzosuberone, ellipticine, and C₆₀ (Sigma-Aldrich, St. Louis MO, U.S.A.). Petroleum crude oil samples and deposits included 400–425 °C and 500–538 °C distillation cuts from Athabasca bitumen heavy vacuum gas oil (HVGO), a sodium naphthenate emulsion, and an extract from a calcium naphthenate deposit.

A working solution of each model compound (10 mM) in toluene was spotted onto a microscope slide (2 μL , ~20 mm diameter spot size) and air-dried prior to analysis. An equimolar mixture consisting of 1.4 mM of each of the following model compounds—5- α cholestane, farnesene, coronene, carbazole, ellipticine, benzodiphenylene sulfide, and dibenzosuberone—was also evaluated. That solution was diluted to a final concentration of 10 μM for each model compound (in 49.5:49.5:1 (v/v/v) toluene/methanol/formic acid) for comparison to electrospray ionization. Each Athabasca bitumen HVGO distillate was spotted (2 μL) at a concentration of 2 mg/mL. The sodium naphthenate emulsion (5 mg) was smeared onto a glass slide directly without any pretreatment, whereas 2 μL of a 2 mg/mL extract²⁶ from the calcium naphthenate deposit in dichloromethane was spotted onto a microscope slide and air-dried prior to analysis.

LD/APPCI Ion Source. Figure 1 is a schematic diagram of the LD/APPCI source interfaced to a custom-built 9.4 T FTICR mass spectrometer.²⁷ The source consists of a sample-coated microscope slide (Gold Seal Products, Portsmouth, NH, U.S.A.) sandwiched in a groove between two stainless steel pieces and fastened by four set screws. The assembly is mounted by posts onto an x - y - z translation stage (Thorlabs, Newton, NJ, U.S.A.) in front of the heated metal capillary (HMC) of the mass spectrometer, with the sample spot positioned <1 mm from the inlet. The sample-coated glass slide is irradiated from the back side by a 355 nm, <150 μm diameter, Q-switched Nd:YAG laser beam (Surelite II, Continuum Inc., Santa Clara, CA., Figure 1, top, pulse width = 4–6 ns, pulse energy ~100 mJ) at frequency of 10 Hz and laser power density, 0.4×10^9 – $2.0 \times 10^9 \text{ W/cm}^2$ unless stated otherwise.

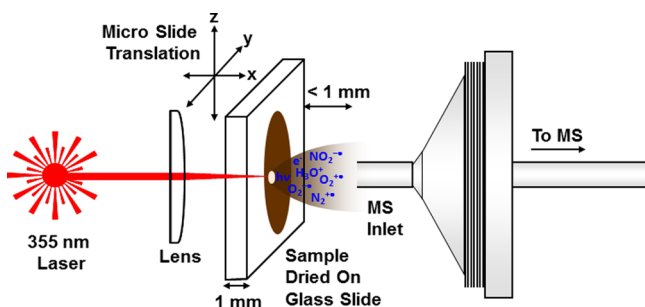


Figure 1. Schematic diagram of a transmission geometry laser desorption atmospheric pressure photochemical ionization (LD/APPCI) source coupled to a linear ion trap mass spectrometer. The source was also interfaced to a 9.4 T FTICR mass spectrometer in the same configuration.

Linear Ion Trap Mass Spectrometry (LIT MS). Initial LD/APPCI source optimization and characterization experiments were performed with positive and negative ions measured by a linear quadrupole ion trap mass analyzer (LTQ, Thermo Finnigan San Jose CA, U.S.A.). Typical instrument parameters were as follows: capillary voltage, 50 V; capillary temperature, 350 °C (unless stated otherwise). The tube lens voltage was 25 V. Data were acquired and processed by use of Xcalibur version 2.0 software (Thermo Fisher Scientific, San Jose, CA, U.S.A.). Each mass spectral scan consisted of three microscans, 100 ms maximum ion injection period generated from an estimated 10 laser shots.

9.4 T FTICR Mass Spectrometry and Data Analysis. Crude oil distillate fractions and deposits were analyzed with a custom-built 9.4 T FTICR mass spectrometer²⁸ with positive and negative ions generated by LD/APPCI. Similar analysis of the distillate fractions was performed by electrospray ionization (ESI) for comparison. A Predator data system was used to collect and process ICR data.²⁹ Ions generated at atmospheric pressure by either LD/APPCI or ESI are introduced into a heated metal capillary and transferred as already reported^{27,30} into an ICR cell for mass analysis. In the ICR cell, the ions are frequency-sweep excited (720–100 kHz, 50 Hz/ μ s, and 360 V_{p-p} amplitude) to \sim 40% of the cell radius, followed by broadband detection, with their postexcitation radii distributed over a range to minimize ion–ion interactions for ultrahigh mass resolution and enhanced dynamic range.³¹ A total of 10–40 individual transients of 5.6 s duration were acquired for each sample and averaged, apodized with a full-Hanning weight function, and zero-filled once prior to fast Fourier transformation. ICR frequencies were converted to ion masses based on the quadrupolar trapping potential approximation.^{32,33} Each mass spectrum was internally calibrated with respect to an abundant homologous alkylation series whose members differ in mass by integer multiples of 14.10565 Da (mass of CH₂) confirmed by isotopic fine structure based on the “walking” calibration equation.³⁴ For each elemental composition, C_cH_hN_nO_oS_s, the heteroatom class, type (double-bond equivalents, DBE = number of rings plus double bonds involving carbon), and carbon number, *c*, were tabulated for subsequent generation of heteroatom class relative abundance distributions and graphical DBE versus carbon number images.

RESULTS AND DISCUSSION

Ion Source Chemistry. Laser desorption atmospheric pressure photochemical ionization is performed in the ambient

interface of the mass spectrometer in transmission geometry, with the laser aligned with the inlet of the heated metal capillary (see Figure 1). The laser generates abundant reagent ions from room air for chemical ionization of vaporized analytes (Figure 2). In the absence of sample, protonated water clusters

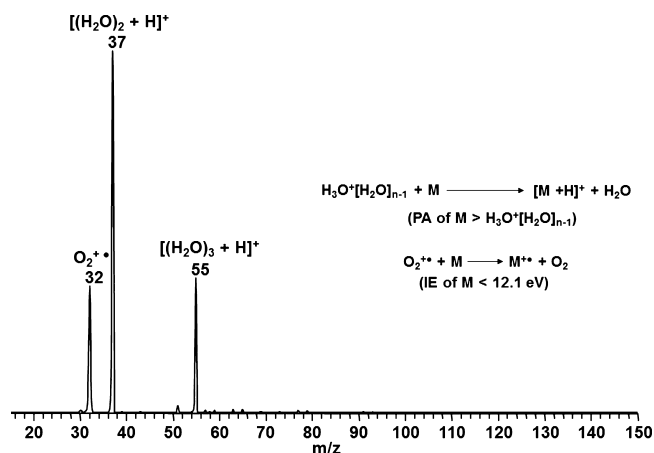


Figure 2. Positive-ion linear ion trap mass spectrum of reagent ions generated from a laser beam passing through a glass slide and aligned with the mass spectrometer inlet capillary in ambient air, in the absence of sample. The proposed reactions are taken from refs 36–38.

((H₂O)_{*n*}H⁺, *n* = 2–3) together with oxygen radical cations (O₂⁺) are the most abundant reagent ion species in the positive linear ion trap mass spectrum (Figure 2). The second harmonic (532 nm) of the Nd:YAG laser results in similar reagent and analyte ion peaks as for 355 nm, but with lower magnitude. Chemical ionization occurs if the gas-phase proton affinity of a vaporized analyte is greater than those for water clusters or if the analyte ionization energy is less than that for O₂. The predominance of small water clusters with lower proton affinity and larger reaction cross section than larger clusters is particularly favorable for efficient proton transfer reactions.^{35–38} Abundant analyte ion signals are observed if the sample is placed very close to the MS inlet (<1 mm). In that region, the plume of desorbed neutral molecules undergoes reactions with reagent ions as they are efficiently drawn into the heated metal capillary, in the absence of ion-accelerating electric fields, to generate analyte ions with minimal fragmentation.^{13,39} Coronene signal magnitude increases with increasing heated metal capillary temperature (up to 450 °C) and laser power density [up to 1.9 × 10⁹ W/cm², with no visible glass slide damage (Supporting Information Figure S1)]. Higher laser power density increases analyte desorption efficiency by some combination of resonant/nonresonant vaporization, depending on the analyte and laser-induced acoustic desorption.^{40,41} The required proximity of the sample to the heated capillary also results in increased radiation-induced thermal desorption of analytes. Higher capillary temperature also increases chemical ionization reaction rates, for higher analyte signal magnitude. Unless stated otherwise, the heated metal capillary temperature was 350 °C and laser power density was 1.5 × 10⁹ W/cm² for all experiments.

Positive Ions. Table 1 presents a summary of the type(s) of positive ions observed for a series of individually ionized petroleum model compounds together with their corresponding limit of detection. Supporting Information Figure S2 shows representative positive-ion mass spectra of various compound

Table 1. Observed Ions, Their Associated Relative Abundances, and Detection Limits for Several Individual Petroleum Model Compounds by Positive-Ion LD/APPCI Linear Ion Trap MS

Name	MW	Structure	Observed Ions	Abundance (%)	Detection Limit (pmol)
Farnesene	204		[M+H] ⁺ M ^{+•}	100 5	0.7
Squalene	410		[M+H] ⁺	100	0.9
Tetradecahydroanthracene	192		[M-H] ⁺	100	1.4
5-alpha cholestane	372		M ^{+•} [M-H] ⁺	100 51	2.0
Perylene	252		[M+H] ⁺ M ^{+•}	100 21	0.4
Benzo(ghi)perylene	276		[M+H] ⁺ M ^{+•}	100 23	0.4
Coronene	300		[M+H] ⁺ M ^{+•}	100 75	0.5
Tetradecylpyrene	762		[M+H] ⁺ M ^{+•}	100 48	0.7
Dodecyl sulfide	370		[M+H] ⁺	100	0.6
Benzodiphenylene sulfide	234		[M+H] ⁺ M ^{+•}	100 14	0.6
Dibenzosuberone	208		[M+H] ⁺	100	0.2
Carbazole	167		[M+H] ⁺ M ^{+•}	100 18	0.5
Ellipticine	246		[M+H] ⁺	100	0.2

classes observed by LD/APPCI, including most of the compounds presented in Table 1. LD/APPCI enables analysis of heteroatom-containing hydrocarbons and nonpolar hydrocarbons, including olefins, polyaromatic hydrocarbons (PAH), saturated hydrocarbons, and even fullerenes (e.g., C₆₀). [M + H]⁺ dominates the mass spectra for heteroatom-containing hydrocarbons due to protonated water cluster reagent ions available for proton transfer reactions with those analytes. The introduction of vaporized D₂O in the region between the sample-containing microscope slide and the MS inlet resulted in abundant [M + D]⁺ ions for ellipticine (Supporting Information Figure S3), verifying that protonated water clusters

are responsible for proton transfer reactions with analytes of higher gas-phase proton affinity. [M + H]⁺ also dominates the mass spectra for olefins and PAHs, presumably due to self-protonation reactions.⁴¹ The PAHs also exhibit M^{+•} species for which ionization efficiency increases with a decrease in ionization energy of the analyte. M^{+•} dominates the mass spectrum for fullerenes (C₆₀). Saturated hydrocarbons are observed as M^{+•} and/or [M - H]⁺, generated by charge exchange with oxygen radical cations or by further reaction of M^{+•} with O₂ by hydrogen atom abstraction.⁴² The limit of detection largely depends on the ionization efficiency of the analyte: the heteroatom-containing analytes, PAHs, and olefins

show limits of detection below 1 pmol, compared to higher limits of detection for saturated hydrocarbons (2 pmol for 5- α cholestane and 1.4 pmol for tetradecahydroanthracene).

Negative Ions. The most abundant reagent ions observed by negative-ion linear ion trap MS include O_2^- , NO_2^- , CO_3^- , HCO_3^- , and HCO_4^- (Supporting Information Figure S4). O_2^- has the largest gas-phase basicity among all of the negative reagent ions⁴³ and undergoes proton transfer reactions to generate $[M - H]^-$ for analytes of lower gas-phase basicity. $[M - H]^-$ is the predominant species observed for pyrrolic nitrogen-containing petroleum model compounds, carbazole and ellipticine (Supporting Information Figure S5, parts a and b). Electron capture is another dominant ionization channel for generating negative ions in LD/APPCI and is commonly observed for compounds of more positive electron affinity than O_2 . M^- predominates the mass spectrum for various model compounds, including dibenzosuberone and C_{60} (Supporting Information Figure S5, parts c and d).

Simple Mixtures. Figure 3, top, shows the positive-ion LD/APPCI mass spectrum from an equimolar mixture of saturated,

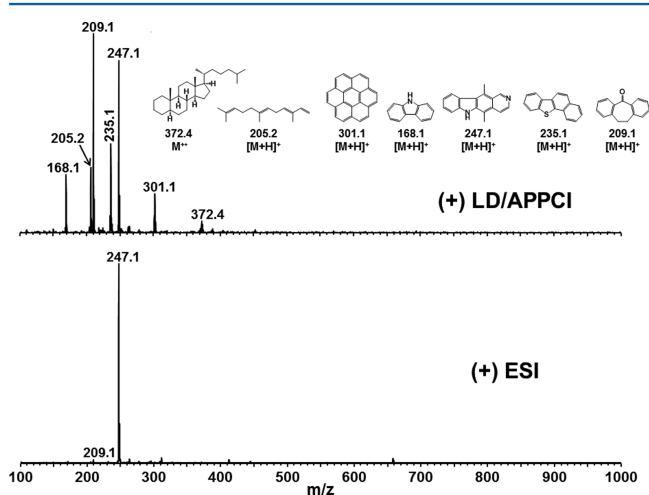


Figure 3. Top: positive-ion linear ion trap mass spectrum of an equimolar mixture (2 μ L of 1.4 mM each) of seven petroleum model compounds: 5- α cholestane, farnesene, coronene, carbazole, ellipticine, benzodiphenylene sulfide, and dibenzosuberone by LD/APPCI. Bottom: ESI mass spectrum of the same sample with each component present at 5 μ M in 50:50 (v/v) toluene/MeOH, 0.1% HCOOH.

olefinic, polyaromatic, and heteroatom-containing (with pyrrolic/pyridinic, thiophenic, and keto functionality) hydrocarbons. Analysis of the same mixture by positive-ion ESI is shown in Figure 3, bottom. All sample components are observed by LD/APPCI MS, mainly as the protonated molecule, except for cholestane which is detected as the molecular radical cation. The various analytes exhibit different relative abundances due to their different gas-phase proton affinity or ionization energy. In contrast, the ESI mass spectrum is dominated by protonated pyridinic nitrogen-containing ellipticine (m/z 247.1), with a minor peak corresponding to protonated dibenzosuberone (m/z 209.1). No other sample components are observed by ESI due to the well-known ion suppression effect that is largely minimized in positive-ion LD/APPCI (due to the availability of multiple ionization channels including protonation, charge exchange, hydride abstraction, etc.). Like APPI (see below),⁴⁴ LD/APPCI thus offers a more general approach for chemical fingerprinting of complex

organic mixtures of compounds spanning a broad range of polarity.

Petroleum Distillates. Athabasca bitumen heavy vacuum gas oil distillates present some of nature's most complex organic mixtures within a dynamic range of $\sim 10\,000$. LD/APPCI is particularly advantageous for analysis of petroleum because many of its components absorb UV laser light, thereby facilitating desorption/ionization with minimal fragmentation of fragile components. The source was coupled to a 9.4 T FTICR mass spectrometer to provide ultrahigh resolution and mass accuracy to enable unambiguous simultaneous determination of the thousands of chemical species present in the samples. Figure 4, top, shows the broad-band positive-ion LD/APPCI mass spectrum of a 500–538 $^{\circ}$ C distillate fraction. The spectrum contains more than 5000 peaks in the range of $200 < m/z < 900$ (each with signal magnitude greater than 6σ of the baseline noise) at a mass resolving power ($m/\Delta m_{50\%}$, in which $\Delta m_{50\%}$ is the full mass spectral peak width at half-maximum peak height) of 699 000 at m/z 500. The molecular weight distribution is centered at m/z 550. The mass resolution is more than sufficient to distinguish between peaks differing by only 3.4 mDa in mass (corresponding to a difference in elemental composition of C_3 versus SH_4 , as seen in Figure 4, top, inset), for confident elemental composition assignments. The validity of the LD/APPCI FTICR MS molecular weight distribution was confirmed by the similar distribution (centered at m/z 556, data not shown) from LD/APPCI with a linear quadrupole ion trap mass spectrometer. That molecular weight distribution is in very good agreement with previously reported ESI, APPI, and FD analysis of the same sample.^{45–47} Finally, LD/APPCI FTICR MS analysis of a lower-boiling fraction (400–425 $^{\circ}$ C) resulted in a molecular weight distribution centered at m/z 375, much lower than for the 500–538 $^{\circ}$ C fraction due to the expected lower m/z for lower cut temperature (Supporting Information Figure S6).

Figure 4, bottom, shows the heteroatom class distribution for all ions higher than 1% relative abundance in the positive-ion LD/APPCI FTICR mass spectrum for the 500–538 $^{\circ}$ C distillate fraction, along with ESI FTICR results for the same sample. Compounds containing one nitrogen atom (N_1) were the most abundant with both ionization techniques, followed by N_1S_1 and N_1O_1 classes. The relative abundance of the N_1 class is slightly higher by ESI, which efficiently ionizes the basic pyridinic nitrogen-containing species. For that class, LD/APPCI generates ions for compounds containing both pyridinic and pyrrolic nitrogen (Figure 3, top).⁴⁸ All of the polar classes generally show similar ionization efficiency by both LD/APPCI and ESI; however, the nonpolar classes such as HC (hydrocarbon), S_1 , and S_2 are observed only by LD/APPCI, consistent with the model compound data (Figure 3), but requiring minimal sample preparation, with the desorption/ionization of samples occurring in one step, simplifying the experiment to provide rapid throughput.

Crude Oil Naphthenate Deposits. Crude oil naphthenates are formed by interaction between saturated acyclic and cycloaliphatic carboxylic acids in petroleum with monovalent (Na^+ , K^+) and divalent (Ca^{2+} , Mg^{2+} , Fe^{2+}) ions in produced water, resulting in emulsion-like and solid deposits generally referred to as sodium naphthenates and calcium naphthenates.^{26,44} These deposits are formed mainly during upstream operations at the oil/water cutoff point, resulting in obstruction of pipelines/screens, production irregularities, and emergency/expensive shutdowns.⁴⁹ The characterization of this material by

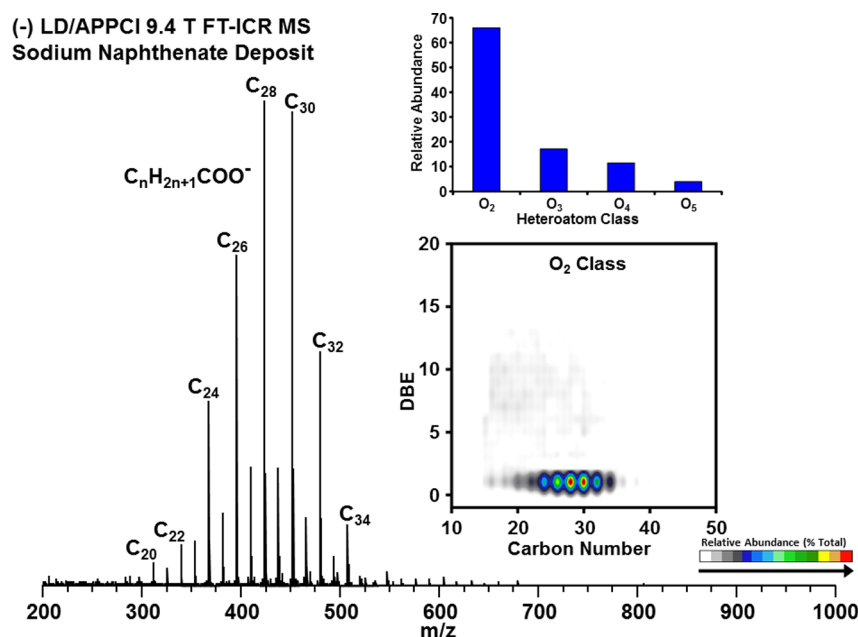


Figure 6. Broad-band negative-ion LD/APPCI 9.4 T FTICR mass spectrum of a sodium naphthenate emulsion from a South American crude oil (ref 26). The top inset is the heteroatom class distribution plot for classes with relative abundance greater than 1%. The bottom inset is the isoabundance-contoured plot of double-bond equivalents vs carbon number for members of the O_2 class.

Figure 6 shows the negative-ion LD/APPCI FTICR mass spectrum obtained from an ~ 5 mg droplet of sodium naphthenate emulsion²⁶ smeared onto a glass target. The mass spectrum ranges from m/z 200 to 700. The inset (Figure 6, top right) shows the heteroatom class distribution for species greater than 1% relative abundance, consisting of O_2 – O_5 compounds. The most abundant class is O_2 , dominated by species of DBE = 1 (Figure 6, bottom inset), namely, saturated straight-chain carboxylic acids with general formula $C_nH_{2n+1}COOH$, $n = 15$ – 36 , spanning a wider range than observed by ESI.²⁶ Lower-abundance carboxylic acids up to DBE 14 are also observed for that class by LD/APPCI, most of which are not observed by ESI (DBE > 5),²⁶ probably due to ionization suppression or loss during sample extraction steps prior to ESI analysis. The higher abundance of the saturated acyclic carboxylic acids in the emulsion is due to their surfactant-like character, which increases their ability to bind monovalent cations in oil/salt water media.²⁶ The generation of negative ions with LD/APPCI is, however, largely due to photochemical ionization processes (vide supra).

CONCLUSION

We present LD/APPCI MS as a novel approach for analysis of complex organic mixtures without the need for matrix, discharges, secondary electrospray, photons, or solvents/vaporizers. The technique provides multiple ionization channels which enable simultaneous analysis of saturated, unsaturated, and heteroatom-containing hydrocarbons. The source also simultaneously generates positive and negative ions without changing any source settings, as for APPI, thereby providing rapid analysis of acid and basic constituents, but without the need for solvents or heat. The absence of matrix interferences makes LD/APPCI MS particularly useful relative to MALDI and related techniques for analysis of small molecules (<2000 Da) in complex organic mixtures such as petroleum crude oil and deposits.

We have coupled LD/APPCI to a 9.4 T FTICR mass spectrometer and demonstrated complex mixture analysis of Athabasca bitumen heavy vacuum gas oil distillates. For example, a 500–538 °C fraction yielded more than 5000 peaks from m/z 200–900, with mass resolving power ($m/\Delta m_{50\%}$, in which $\Delta m_{50\%}$ is the full mass spectral peak width at half-maximum peak height) of $\sim 700\,000$ at m/z 500, for simultaneous characterization of polar and nonpolar components. Application to a calcium naphthenate deposit and a sodium naphthenate emulsion (with no sample pretreatment) resulted in a more comprehensive compositional fingerprint than obtained by ESI. Our current efforts are geared toward a detailed evaluation of the ionization mechanism(s).

ASSOCIATED CONTENT

Supporting Information

Additional information as noted in text. This material is available free of charge via the Internet at <http://pubs.acs.org>.

AUTHOR INFORMATION

Corresponding Authors

*Phone: +1 850-644-2398. Fax: +1 850-644-1366. E-mail: rodgers@magnet.fsu.edu.

*Phone: +1 850-644-0529. Fax: +1 850-644-1366. E-mail: marshall@magnet.fsu.edu.

Present Addresses

^{||}L.N.: Phillips 66 Company, 266-A PL, PRC, Bartlesville, OK 74003-6670, United States.

[†]M.M.M.: Schlumberger DBR Technology Center, 9450 17 Avenue, Edmonton, Alberta, T6N 1M9, Canada.

Notes

The authors declare no competing financial interest.

ACKNOWLEDGMENTS

This work was supported by NSF Division of Materials Research through DMR-11-57490 and the State of Florida. The

authors thank John P. Quinn and Daniel G. McIntosh for assistance with fabrication of the sample probe.

REFERENCES

- (1) Caprioli, R. M.; Farmer, T. B.; Gile, J. *Anal. Chem.* **1997**, *69*, 4751.
- (2) Karas, M.; Hillenkamp, F. *Anal. Chem.* **1988**, *60*, 2299.
- (3) Tanaka, K.; Waki, H.; Ido, Y.; Akita, S.; Yoshida, Y.; Yoshida, T. *Rapid Commun. Mass Spectrom.* **1988**, *2*, 151.
- (4) Zenobi, R.; Knochenmuss, R. *Mass Spectrom. Rev.* **1998**, *17*, 337.
- (5) Laiko, V. V.; Moyer, S. C.; Cotter, R. J. *Anal. Chem.* **2000**, *72*, 5239.
- (6) Moyer, S. C.; Cotter, R. J.; Woods, A. S. *J. Am. Soc. Mass Spectrom.* **2002**, *13*, 274.
- (7) Trimpin, S.; Inutan, E. D.; Herath, T. N.; McEwen, C. N. *Anal. Chem.* **2010**, *82*, 11.
- (8) Navare, A.; Nouzova, M.; Noriega, F. G.; Hernandez-Martinez, S.; Menzel, C.; Fernandez, F. M. *Rapid Commun. Mass Spectrom.* **2009**, *23*, 477.
- (9) Lewis, W. G.; Shen, Z. X.; Finn, M. G.; Siuzdak, G. *Int. J. Mass Spectrom.* **2003**, *226*, 107.
- (10) Laiko, V. V.; Taranenko, N. I.; Berkout, V. D.; Musselman, B. D.; Doroshenko, V. M. *Rapid Commun. Mass Spectrom.* **2002**, *16*, 1737.
- (11) Posthumus, M. A.; Kistemaker, P. G.; Meuzelaar, H. L. C.; Tennoeverdebrauw, M. C. *Anal. Chem.* **1978**, *50*, 985.
- (12) Zhan, Q.; Wright, S. J.; Zenobi, R. *J. Am. Soc. Mass Spectrom.* **1997**, *8*, 525.
- (13) Coon, J. J.; McHale, K. J.; Harrison, W. W. *Rapid Commun. Mass Spectrom.* **2002**, *16*, 681.
- (14) Herdering, C.; Reifschneider, O.; Wehe, C. A.; Sperling, M.; Karst, U. *Rapid Commun. Mass Spectrom.* **2013**, *27*, 1.
- (15) Kolaitis, L.; Lubman, D. M. *Anal. Chem.* **1986**, *58*, 2137.
- (16) Galhena, A. S.; Harris, G. A.; Nyadong, L.; Murray, K. K.; Fernandez, F. M. *Anal. Chem.* **2010**, *82*, 2178.
- (17) Nemes, P.; Vertes, A. *Anal. Chem.* **2007**, *79*, 8098.
- (18) Rezenom, Y. H.; Dong, J.; Murray, K. K. *Analyst* **2008**, *133*, 226.
- (19) Cheng, C. Y.; Yuan, C. H.; Cheng, S. C.; Huang, M. Z.; Chang, H. C.; Cheng, T. L.; Yeh, C. S.; Shiea, J. *Anal. Chem.* **2008**, *80*, 7699.
- (20) Ovchinnikova, O. S.; Kertesz, V.; Van Berkel, G. J. *Rapid Commun. Mass Spectrom.* **2011**, *25*, 3735.
- (21) Brady, J. J.; Judge, E. J.; Levis, R. J. *Rapid Commun. Mass Spectrom.* **2009**, *23*, 3151.
- (22) Vaikkinen, A.; Shrestha, B.; Kauppila, T. J.; Vertes, A.; Kostianen, R. *Anal. Chem.* **2012**, *84*, 1630.
- (23) Raffaelli, A.; Saba, A. *Mass Spectrom. Rev.* **2003**, *22*, 318.
- (24) Constapel, M.; Schellentrager, M.; Schmitz, O. J.; Gab, S.; Brockmann, K. J.; Giese, R.; Benter, T. *Rapid Commun. Mass Spectrom.* **2005**, *19*, 326.
- (25) Robb, D. B.; Covey, T. R.; Bruins, A. P. *Anal. Chem.* **2000**, *72*, 3653.
- (26) Mapolelo, M. M.; Stanford, L. A.; Rodgers, R. P.; Yen, A. T.; Debord, J. D.; Asomaning, S.; Marshall, A. G. *Energy Fuels* **2009**, *23*, 349.
- (27) Kaiser, N. K.; Savory, J. J.; McKenna, A. M.; Quinn, J. P.; Hendrickson, C. L.; Marshall, A. G. *Anal. Chem.* **2011**, *83*, 6907.
- (28) Kaiser, N. K.; Quinn, J. P.; Blakney, G. T.; Hendrickson, C. L.; Marshall, A. G. *J. Am. Soc. Mass Spectrom.* **2011**, *22*, 1343.
- (29) Blakney, G. T.; Hendrickson, C. L.; Marshall, A. G. *Int. J. Mass Spectrom.* **2011**, *306*, 246.
- (30) Tolmachev, A. V.; Robinson, E. W.; Wu, S.; Kang, H.; Lourette, N. M.; Pasa-Tolic, L.; Smith, R. D. *J. Am. Soc. Mass Spectrom.* **2008**, *19*, 586.
- (31) Kaiser, N. K.; McKenna, A. M.; Savory, J. J.; Rodgers, R. P.; Hendrickson, C. L.; Marshall, A. G. *Anal. Chem.* **2013**, *85*, 265.
- (32) Ledford, E. B. J.; Rempel, D. L.; Gross, M. L. *Anal. Chem.* **1984**, *56*, 2744.
- (33) Shi, S. D. H.; Drader, J. J.; Freitas, M. A.; Hendrickson, C. L.; Marshall, A. G. *Int. J. Mass Spectrom.* **2000**, *195*, 591.
- (34) Savory, J. J.; Kaiser, N. K.; McKenna, A. M.; Xian, F.; Blakney, G. T.; Rodgers, R. P.; Hendrickson, C. L.; Marshall, A. G. *Anal. Chem.* **2011**, *83*, 1732.
- (35) Kawai, Y.; Yamaguchi, S.; Okada, Y.; Takeuchi, K. *J. Mass Spectrom. Soc. Jpn.* **2004**, *52*, 271.
- (36) Kawai, Y.; Yamaguchi, S.; Okada, Y.; Takeuchi, K.; Yamauchi, Y.; Ozawa, S.; Nakai, H. *Chem. Phys. Lett.* **2003**, *377*, 69.
- (37) Nyadong, L.; Galhena, A. S.; Fernandez, F. M. *Anal. Chem.* **2009**, *81*, 7788.
- (38) Xiaolin, Y.; Castleman, A. W., Jr. *J. Am. Chem. Soc.* **1989**, *111*, 6845.
- (39) Peng, S.; Ahlmann, N.; Kunze, K.; Nigge, W.; Edler, M.; Hoffmann, T.; Franzke, J. *Rapid Commun. Mass Spectrom.* **2004**, *18*, 1803.
- (40) Lindner, B.; Seydel, U. *Anal. Chem.* **1985**, *57*, 895.
- (41) Nyadong, L.; McKenna, A. M.; Hendrickson, C. L.; Rodgers, R. P.; Marshall, A. G. *Anal. Chem.* **2011**, *83*, 1616.
- (42) Nyadong, L.; Quinn, J. P.; Hsu, C. S.; Hendrickson, C. L.; Rodgers, R. P.; Marshall, A. G. *Anal. Chem.* **2012**, *84*, 7131–7137.
- (43) Song, L. G.; Dykstra, A. B.; Yao, H. F.; Bartmess, J. E. *J. Am. Soc. Mass Spectrom.* **2009**, *20*, 42.
- (44) Mapolelo, M. M.; Rodgers, R. P.; Blakney, G. T.; Yen, A. T.; Asomaning, S.; Marshall, A. G. *Int. J. Mass Spectrom.* **2011**, *300*, 149.
- (45) McKenna, A. M.; Purcell, J. M.; Rodgers, R. P.; Marshall, A. G. *Energy Fuels* **2010**, *24*, 2929.
- (46) Smith, D. F.; Rahimi, P.; Teclerariam, A.; Rodgers, R. P.; Marshall, A. G. *Energy Fuels* **2008**, *22*, 3118.
- (47) Smith, D. F.; Schaub, T. M.; Kim, S.; Rodgers, R. P.; Rahimi, P.; Teclerariam, A.; Marshall, A. G. *Energy Fuels* **2008**, *22*, 2372.
- (48) Purcell, J. M.; Hendrickson, C. L.; Rodgers, R. P.; Marshall, A. G. *J. Am. Soc. Mass Spectrom.* **2007**, *18*, 1682.
- (49) Lutnaes, B. F.; Brandal, O.; Sjoblom, J.; Krane, J. *Org. Biomol. Chem.* **2006**, *4*, 616.
- (50) Baugh, T. D.; Wolf, N. O.; Mediaas, H.; Vinstad, J. E.; Grande, K. V. *Prepr.—Am. Chem. Soc., Div. Pet. Chem.* **2004**, 274.
- (51) Baugh, T. D.; Wolf, N. O.; Mediaas, H.; Vinstad, J. E.; Grande, K. V. Presented at the Society of Petroleum Engineers (SPE) 7th International Symposium on Oilfield Scale, Aberdeen, Scotland, May 2005; SPE Paper No. 93011.
- (52) Brandal, O.; Hanneseth, A. M.; Hemmingsen, P. V.; Sjoblom, J.; Kim, S.; Rodgers, R. P.; Marshall, A. G. *J. Dispersion Sci. Technol.* **2006**, *27*, 295.